RESEARCH ARTICLE | FEBRUARY 25 2022

In-plasma photo-assisted etching of Si with chlorine aided by an external vacuum ultraviolet source FREE

Special Collection: Plasma Processing for Advanced Microelectronics

Linfeng Du; Demetre J. Economou ; Vincent M. Donnelly

Check for updates

Journal of Vacuum Science & Technology B 40, 022207 (2022)
https://doi.org/10.1116/6.0001710
CHORUS

View Online
Export Citation
CrossMark

05 September 2023 11:49:35

JVST B
Journal of Vacuum Science & Technology B

ARTICLE

avs.scitation.org/journal/jvb

In-plasma photo-assisted etching of Si with chlorine aided by an external vacuum ultraviolet source

Cite as: J. Vac. Sci. Technol. B 40, 022207 (2022); doi: 10.1116/6.0001710
Submitted: 22 December 2021 · Accepted: 31 January 2022 ·
Published Online: 25 February 2022

View Online Export Citation CrossMark

Linfeng Du, Demetre J. Economou,[a] and Vincent M. Donnelly[b]

AFFILIATIONS

Plasma Processing Laboratory, William A. Brookshire Department of Chemical and Biomolecular Engineering, University of Houston, Houston, Texas 77204

Note: This paper is a part of the Special Topic Collection on Plasma Processing for Advanced Microelectronics.
[a]**Electronic mail:** economou@uh.edu
[b]**Electronic mail:** vmdonnelly@uh.edu

ABSTRACT

Photo-assisted etching of *p*-type Si was previously found to occur in a chlorine-containing, Faraday-shielded, inductively coupled plasma (ICP), and this was attributed to the vacuum ultraviolet (VUV) light generated by the plasma. Other causes for the very high etching rates were ruled out, including ion bombardment. In the present study, the substrate in the main Cl_2/Ar ICP was subjected to extra VUV light that was generated in an independently controlled, auxiliary Ar/He ICP in tandem with the main ICP. The ICPs were separated by a tungsten mesh and a bundle of high-aspect-ratio quartz tubes in a honeycomb configuration. There was no measurable perturbation of the main plasma by the auxiliary plasma. The etching rate was found to be enhanced by 11%–51% with the additional VUV light provided by the auxiliary ICP. With absolute measurements of the auxiliary ICP photon flux at the sample surface, as described elsewhere, incredibly large etching yields of 90–240 Si atoms per photon were obtained. It is argued that etching is not a result of electron–hole pair formation but is instead ascribed to a photocatalytic chain reaction.

Published under an exclusive license by the AVS. https://doi.org/10.1116/6.0001710

05 September 2023 11:49:35

I. INTRODUCTION

Silicon etching with chlorine-containing plasmas continues to play pivotal roles in the manufacturing of advanced silicon integrated circuits.[1] Although great progress has been and is being made in this area, new challenges arise as critical dimensions of devices approach the atomic scale and self-limiting atomic layer etching (ALE) processes gain acceptance.[2] The fastest ALE rates call for efficient surface chlorination in a Cl-atom-generating plasma, with very low-energy ion bombardment to minimize etching during this step. The product removal step, induced by ion bombardment, is also optimally carried out at low ion energies to minimize amorphization of surface and subsurface chlorination.

One complication in etching with low-energy ions is competing etching, which has been attributed to light generated by the plasma.[3–7] While studying the etching of *p*-type silicon in high-density (a positive ion density of 10^{12} cm^{-3}) Cl_2/Ar plasmas that produced very low-energy ions (~10 eV), Shin *et al.* discovered that substantial etching occurred.[3] After ruling out other potential etching mechanisms, they concluded that vacuum ultraviolet (VUV) photons produced in the plasma were contributing to extremely efficient photo-assisted etching (PAE).

Many researchers have reported on the photon-induced/enhanced etching of semiconductor materials in a halogen gas atmosphere in the *absence of a plasma*. Photodissociation of Cl_2 occurs in the gas phase at wavelengths less than 500 nm, and Okano *et al.* found that n^+ poly-Si could be etched isotopically with Cl atoms produced by photodissociation.[8] However, semi-insulating and *p*-type Si required Cl atoms (produced by photodissociation of Cl_2) *plus* surface irradiation with UV or visible light for etching to occur. They attributed etching to the creation of electron–hole pairs that promoted surface reactions.[8] In similar studies by Kullmer and Bäuerle, Cl atoms were generated above p-type Si

Published under an exclusive license by the AVS

(1.1×10^{14} cm^{-3} B-doped) by photodissociation of Cl_2 with a 308 nm XeCl laser (parallel to the surface) while irradiating the substrate with normal incidence light at 647.1 nm (cw Kr^+ laser).[9] They found that the etching rate increased in proportion to the Cl flux and also increased with Kr^+ laser fluence to a power of 0.7. They attributed etching to photogenerated carriers. Sesselmann *et al.* studied laser-induced chemical etching of Si (100) in Cl_2 by using a pulsed excimer laser at 308 and 248 nm.[10] They attributed the wavelength dependence at low laser fluence to photodissociation of Cl_2 gas and the efficient photodesorption of silicon chlorides. Jackman *et al.* showed that UV irradiation could modify the surface silicon chlorides into a weaker bonding state, leading to enhanced rates of desorption of $SiCl_4$ upon heating.[11]

Schwentner and co-workers investigated photo-assisted etching Si in the presence of XeF_2 vapors as well as GaAs with Cl_2.[12,13] In both cases, the number of Si atoms etched per photon dramatically increased below about 130 nm and reached an incredible ~100 between 130 and 110 nm. Furthermore, they argued that since most photons penetrated more deeply, the efficiency per absorbed photon at the surface was of the order of 10^5 Si atoms per photon. Such yields far in excess of unity were attributed to unspecified chain reactions.

In our previous studies, in-plasma photo-assisted etching below the ion-assisted etching (IAE) energy threshold was shown to be mainly due to VUV photons with wavelengths <120 nm, where among possible mechanisms are photon-induced lattice damage or carrier-mediated reactions.[3,4] When a Cl_2/Ar plasma was modulated between high and low plasma powers at 1 kHz, the spontaneous etching rate, monitored through the Si-to-Ar and SiCl-to-Ar emission intensity ratio, was also modulated.[5] This indicates that a prompt process such as photon-generated electron–hole pairs or photon-stimulated desorption is responsible for etching and not lattice damage, which will modulate on a much longer time scale required to etch several monolayers of potentially damaged Si.

PAE could be reduced by energetic ion bombardment, which amorphizes the surface.[6] This was proposed to enhance the recombination of electron–hole pairs that otherwise would participate in etching reactions, though other possible explanations can also be envisioned. Moreover, PAE could be suppressed by adding small amounts of oxygen to the plasma, leading to the formation of a silicon oxide layer that suppressed PAE, while IAE continued uninhibited.[7] In all these studies, the VUV light source was the plasma itself. Thus, the VUV photon intensity and wavelengths were constrained by the plasma (e.g., power, pressure, gas composition, flow rate, etc.). An estimate of 0.8 Si per photon was made for etching in a 50%Cl_2/Ar inductively coupled plasma (ICP).[3] This was based on the assumption that the VUV photon flux would be the same as that reported for a pure Ar ICP of similar power density and pressure. More recently, it was shown, however, that the total VUV flux from a 50% Cl_2/Ar ICP was about 100 times less than that in an Ar ICP.[14] This would mean that the PAE yields in the experiments by Shin *et al.*[3] were closer to 100, i.e., similar to those reported by Schwentner and co-workers[13,15] for Si and GaAs etching in the presence of VUV light with XeF_2 and Cl_2, respectively.

In this work, to better control and quantify the VUV photon flux density and wavelength, an independent ICP VUV source (*auxiliary ICP*) was installed in tandem with the main ICP. The effect of the additional VUV flux, generated by Ar/He plasmas in the auxiliary ICP, on the etching of *p*-type Si in Ar/Cl_2 plasmas in the main ICP was studied (in the absence of energetic ion bombardment). A scanning electron microscope (SEM) was used to examine the surface morphology of etched samples and to determine the etched depth and, thus, the etching rate. X-ray photoelectron spectroscopy (XPS), with sample transfer under vacuum, was used to study surface composition. In work reported elsewhere,[16] the absolute VUV photon flux on the Si sample was measured *in situ* by recording photoemission currents from a Au-coated Cu sensor, and etching yields (Si atoms per photon) were obtained.

II. EXPERIMENT

The experimental apparatus is shown schematically in Fig. 1. The Faraday-shielded main (lower) ICP was generated in an alumina tube (33.0 -cm long, 7.94 -cm inside diameter) powered by a four-turn air-cooled copper coil. The 13.56 MHz continuous wave power produced by a function generator (Keysight, 33 600A) and an RF amplifier (ENI A500) was supplied to the main ICP through a Π-matching network. The net (forward minus reflected), nominal ICP power was in the range of 60–350 W. The sample

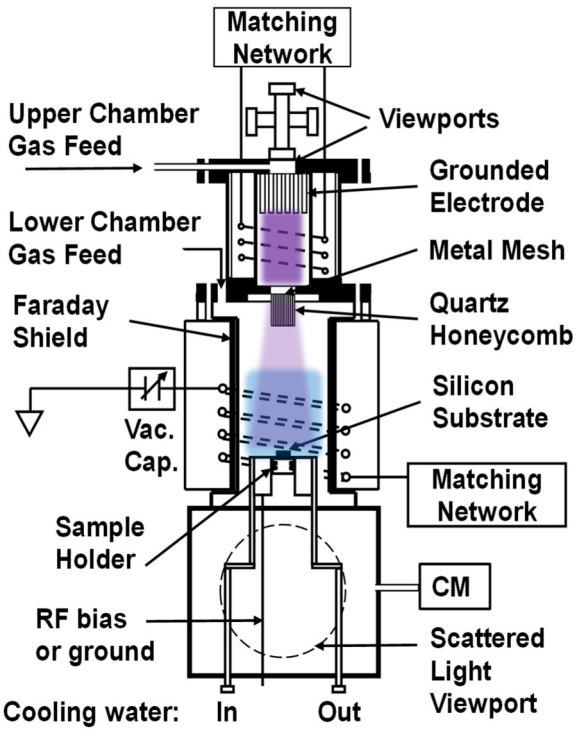

FIG. 1. Schematic of the main (lower) ICP in tandem with the auxiliary (upper) ICP (VUV source). The two ICPs were separated by a grounded tungsten mesh and a 3-cm-long quartz honeycomb. The sample stage was 30 cm away from the lower end of the honeycomb. A single turbomolecular pump below the main ICP (not shown) evacuated both ICPs. CM = capacitance manometer.

05 September 2023 11:49:35

Published under an exclusive license by the AVS

holder could be briefly RF-powered to generate a DC self-bias for native oxide removal, but otherwise, the sample holder was grounded. The 13.56 MHz RF bias was produced by a function generator (Stanford Research Systems, DS345) and an RF amplifier (ENI, A150). Details of the main ICP reactor can be found elsewhere.[6,7]

The auxiliary ICP reactor (19.5 -cm long, 3.56 -cm inside diameter water-cooled alumina tube) was powered at 13.56 MHz, produced by a function generator (BNC, Model 645), an RF amplifier (ENI, A150), and a T-matching network. Argon (Matheson, 99.999% purity) at 25 SCCM or He (Advanced Specialty Gases, 99.999% purity) and Ar-mixed gas at 50 SCCM (regulated by mass flow controllers MKS Model 1179A) was fed to the auxiliary ICP. The two ICPs were mostly operated in a "free-running" mode, with no locking of the phases of the 13.56 MHz sources. In several cases, a single function generator was used to drive both RF power amplifiers with a controllable phase difference.

The auxiliary ICP source was separated from the main ICP source by a grounded tungsten mesh (230 μm square openings, 81% transparency), followed by a bundle of 31 quartz tubes (each 0.5 cm OD, 0.4 cm ID, 3.0 cm-long) arranged in a honeycomb configuration with a bundle diameter of ~4 cm, providing an open area of ~50%. All of the gas fed into the top of the auxiliary ICP flowed through the honeycomb separator and into the downstream chamber; i.e., the auxiliary source had no pump of its own. The total open area, A_{OA}, through which the gas flows from the auxiliary chamber to the main chamber is, therefore, $0.81 \times 31 \times \pi \times (0.2)^2\ \mathrm{cm}^2 = 3.16\ \mathrm{cm}^2$. A 300 l/s turbomolecular pump (Ebara, ET300W) downstream of the main ICP was used to pump both ICPs. The base pressure measured with an ionization gauge downstream of the main ICP with no gas flow was $\sim 2.0 \times 10^{-7}$ Torr. The pressure in the main ICP with gas flow was measured with a capacitance manometer (MKS 629, 0.1 Torr full scale). The reported pressures in the main and auxiliary ICPs account for the pressure drops from their locations to that of the manometer. The main ICP reactor pressure (P_M = 15–60 mTorr) was changed by either throttling the gate valve just above the turbomolecular pump or adjusting the main gas flow rate. Poiseuille's law with a modification for compressible fluid was used to estimate the pressure in the auxiliary ICP,[16] which for 47.5 SCCM He and 2.5 SCCM Ar flow into the auxiliary source was 277 mTorr when the main source pressure was 60 mTorr and 270 mTorr when the main source pressure was 15 mTorr.

A highly doped blanket *p*-type Si (100) wafer (resistivity 0.001–0.005 Ω cm) was cleaved into $\sim 1.1 \times 1.1\ \mathrm{cm}^2$ samples for postetching XPS measurements. Each sample was cleaned with acetone, methanol, and DI water. Unless otherwise stated, the samples were sputtered for 2 s (RF powered, −65 V DC self-bias) to remove the native oxide before PAE commenced. In a few cases, the native oxide was instead removed by immersion in a 2% HF solution for 1 min. To achieve good thermal and electrical contact, the samples were soldered, under a N_2 atmosphere, on a 1.95 cm-diameter highly doped *p*-type Si cover disk that was soldered onto a 2.54- cm-diameter stainless steel sample holder using an indium foil (0.05 mm-thick, Stanford Advanced Materials, 99.995% purity). The Si cover disk reduced any metal contamination from sputtering of the stainless steel sample holder to below the detection limit for XPS (atomic concentration of <0.5%).

Patterned samples [1 μm-thick SiO_2 lines on a *p*-type Si (100) substrate with a resistivity of 5–100 Ω cm, corresponding to a hole concentration, n_p, of 4×10^{15}–$1 \times 10^{14}\ \mathrm{cm}^{-3}$] were used for studying average etching rates and surface morphology. The pitch width (line + space) of the pattern was 100 μm at 50% density. As with the blanket samples, the patterned samples were cleaned with methanol, acetone, and DI water and soldered with indium onto the Si disk covering the sample holder.

The I-V characteristics of the substrate immersed in the plasma were measured with a DC bias (created by a bank of 9 V and 1.5 V batteries) applied to the substrate. Currents to the substrate were measured for positive and negative voltages using either a multimeter (Fluke 177) for mA-level currents or a picoammeter (Keithley 6485) for μA-level currents.

Line-of-sight light from the auxiliary ICP, as well as light from the main ICP that passed through the honeycomb, was collected through a MgF_2 window (1-in. diameter) at the top of the auxiliary reactor. Scattered light from the main ICP was also recorded through a quartz viewport (4.5-in. diameter) downstream of the main reactor. Optical emission spectra (OES), recorded with a spectrometer (Ocean Optics HR4000 with 1.7 Å resolution), covered the 735–920 nm region. An optical fiber was used to lead light into the spectrometer. The integration time and signal averaging were adjusted according to the intensity.

SEM (FIE XL-30) images of cleaved, masked samples were used to measure etching rates and investigate surface morphology. The XPS system (Surface Science Instruments) used to analyze unmasked samples consisted of an Al K-α (photon energy of 1486.6 eV) monochromatized x-ray source and a hemispherical electron energy analyzer. At a 30° take-off angle, the 1/e probing depth of Si was about 10 Å.[17] Details of the XPS system can be found elsewhere.[6,7] The surface elemental composition was determined by low-resolution survey spectra, scanning the range of 0–1000 eV with an 800 μm-diameter beam diameter.

05 September 2023 11:49:35

III. RESULTS AND DISCUSSION

A. Possible interactions between the auxiliary and the main ICPs

The characterization of the auxiliary ICP, operated in a standalone configuration, has been reported elsewhere.[16] Ar/He plasmas (2.5 SCCM Ar and 47.5 SCCM He) produced the strongest emission from Ar 106.67 nm. Less-intense emission from Ar at 104.82 nm was also observed in addition to weaker emissions from Ar^+ at 92.0 and 93.2 nm. Other still weaker emissions were found, but their total emission intensities were small compared with the sum of the 106.67 and 104.82 nm lines.

Ideally, the two plasmas would be separated by a VUV transmitting window. Unfortunately, no materials are available that are transparent at 106 nm, the wavelengths of the strongest emissions from an Ar plasma. It is, therefore, necessary to separate the two ICPs with a windowless divider such as the grid-honeycomb structure described above.

Published under an exclusive license by the AVS

It is possible that the auxiliary and main ICPs could affect each other by an exchange of charged and neutral species, complicating the interpretations of Si etching caused by the added VUV light from the auxiliary ICP. First, we discuss neutral species exchange due to a back diffusion of gas from the main ICP into the auxiliary ICP. Although all of the auxiliary ICP feed gas flows through the honeycomb into the main ICP, a back diffusion of chlorine and Ar from the main ICP could perturb the spectrum and intensities of the VUV light generated in the auxiliary ICP.

The amount of back diffusion is related to the Péclet number, defined as $Pe = vL/D$, where v is the gas velocity along a tube of length L and D is the diffusion coefficient. When $Pe >> 1$, back diffusion is negligible. The gas speed in each tube is given by

$$v(\text{cm/s}) = \left(\frac{760}{P}\right)\left(\frac{T_g}{273}\right)\frac{f^a_{tot}}{60\,A_{OA}}, \tag{1}$$

where P and T_g are the pressure (Torr) and gas temperature (K) in the auxiliary chamber, f^a_{tot} is the total feed gas flow rate (SCCM) into the auxiliary chamber, and A_{OA} is the open area of the honeycomb available for the gas flow. The diffusion coefficient, D, at pressure P is simply $760\,D_{atm}/P$, where D_{atm} is the diffusion coefficient at atmospheric pressure. While v and D depend on P (which drops along the tubes between the auxiliary and the main chambers), their ratio does not. Assuming a constant temperature along the length of the tube, the Péclet number can be written as

$$Pe = \frac{T^a_g f^a_{tot} L}{16\,380\,A_{OA} D_{atm}}, \tag{2}$$

where all the variables have cgs units. While the numerator depends linearly on T_g, D_{atm} has a dependence of $T_g^{1.5}$; hence, Pe depends only mildly on T_g.

For one set of conditions used below (5 SCCM Cl_2 and 245 SCCM Ar in the main ICP, and 47.5 SCCM He and 2.5 SCCM Ar in the auxiliary ICP), the gas near the downstream exit of the honeycomb was 83% Ar. Using the self-diffusion coefficient for Ar of 0.2 $cm^2\,s^{-1}$ near 350 K,[18] $Pe = 5.1$. At the upstream side of the honeycomb, the gas is mostly He, so using the He-Ar binary diffusion coefficient of 0.96 $cm^2\,s^{-1}$ at 350 K,[19] $Pe = 1.1$. Consequently, the back diffusion of Ar, as well as chlorine, while not negligible, is not expected to be excessive.

To further assess back diffusion, OES was used to observe Cl in the auxiliary ICP. The lower ionization potential of Cl could cause the population of high-energy electrons to be reduced,[20] perhaps leading to a reduction in VUV intensity. The Cl-to-Ar atom number density ratio was estimated using optical emission and the rare gas actinometry relationship,[21–23]

$$\frac{n_{\text{Cl}}}{n_{\text{Ar}}} = a_{\text{Cl,Ar}}\frac{I_{\text{Cl}}}{I_{\text{Ar}}}\frac{\gamma_{\text{Ar}}}{\gamma_{\text{Cl}}}, \tag{3}$$

where n_{Cl} is the Cl number density, n_{Ar} is the total Ar number density, corresponding to the sum of Ar fed to the upstream ICP chamber (n^u_{Ar}) and the Ar that back-diffuses from the downstream chamber (n^d_{Ar}), I_{Cl} and I_{Ar} are the emission line intensities of Cl (792.4 nm) and Ar (750.4 nm), $\alpha_{\text{Cl,Ar}}$ is a proportionality constant ($\alpha_{\text{Cl,Ar}} = 2.1$),[21] and $\gamma_{\text{Ar}}/\gamma_{\text{Cl}}$ is the ratio of spectrometer sensitivity at the corresponding wavelengths ($\gamma_{\text{Ar}}/\gamma_{\text{Cl}} = 1.37$).[21] If it is assumed that the sum of Cl and Cl_2 has a similar diffusivity to that of Ar and further assumed that Cl_2 is 100% dissociated in the ICP (a reasonable assumption at the power density of 1 W/cm^3), then it can be shown that the fraction of Ar in the ICP resulting from Ar back diffusion from the lower chamber is given by

$$\frac{n^d_{\text{Ar}}}{n^u_{\text{Ar}} + n^d_{\text{Ar}}} = a_{\text{Cl,Ar}}\frac{I_{\text{Cl}}}{I_{\text{Ar}}}\frac{\gamma_{\text{Ar}}}{\gamma_{\text{Cl}}}\frac{f_{\text{Ar}}}{2f_{\text{Cl}_2}}. \tag{4}$$

Emission intensities and number density ratios are plotted as a function of the Cl_2 flow rate in the main chamber in Fig. 2 for one typical set of conditions. The $n_{\text{Cl}}/n_{\text{Ar}}$ number density ratio reaches ~0.05 at a Cl_2 flow rate of 25 SCCM into the main chamber. Between 46% and 21% of the Ar in the auxiliary ICP is due to the back-diffused Ar from the main chamber.

This back diffusion reduced the Ar $2p_1 \rightarrow 1s_2$ 750.4 -nm emission intensity by only 12% at the maximum Cl_2 flow rate of 25 SCCM, as shown in Fig. 2. Ar $2p_5 \rightarrow 1s_4$ emission at 751.5 nm behaved similarly (not shown). These emissions are expected to behave in a manner similar to the strong VUV emissions from the $1s_2$ and $1s_4$ states when they decay to the ground state. Therefore, it was concluded that back diffusion had a relatively small effect on the VUV emission under the conditions investigated.

To determine whether charged particles exit the auxiliary ICP, the current through a p-type Si sample was measured as a function

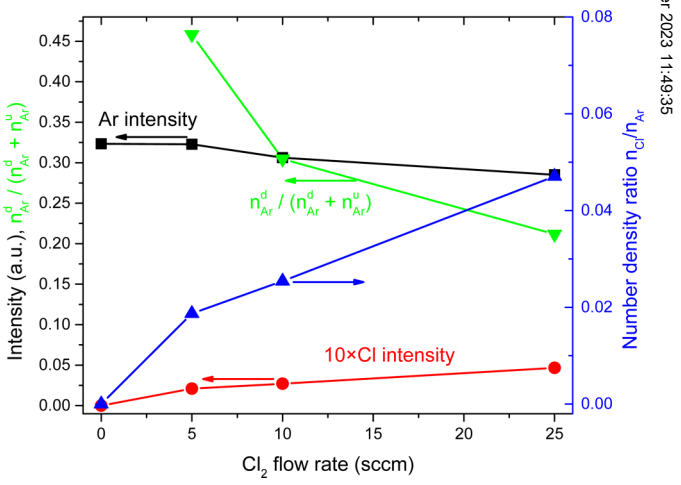

FIG. 2. Ar 750.4 -nm line intensity (black squares) and Cl 792.4 -nm line intensity multiplied by 10 (red circles) as a function of Cl_2 flow rate in the main ICP. Auxiliary ICP feed gases: 47.5 SCCM He and 2.5 SCCM Ar. Main ICP feed gases: 0–25 SCCM Cl_2 and total flow rate of 250 SCCM (Cl_2 + Ar). Measured main ICP pressure = 60 mTorr. Estimated auxiliary ICP pressure = 277 mTorr. Auxiliary ICP power = 200 W. The main ICP was not powered. The Cl-to-Ar number density ratios and fraction of back-diffused Ar in the auxiliary ICP, calculated from Eqs. (3) and (4) (right axis, blue triangles and left axis, green inverted triangles, respectively).

05 September 2023 11:49:35

Published under an exclusive license by the AVS

of the substrate DC bias in the main ICP (Fig. 3). With just the auxiliary ICP on, the positive ion current to the substrate biased at −25 to −50 V DC was about four orders of magnitude smaller than that measured at the same negative bias with only the main ICP on, indicating that very few ions escaped the auxiliary ICP. Also, the ion current measured with both plasmas on was actually slightly *less* (12%) than that with just the main ICP on at 60 W and nearly identical (3% more) at 350 W (not shown), suggesting that the ion density and flux to the substrate in the main ICP was not significantly enhanced by the auxiliary ICP and, therefore, could not be the cause of an increase in the etching rate (in addition to the ion energy being too low).

With only the main ICP powered, near-zero currents were recorded with positive potentials applied to the substrate (Fig. 3) because the plasma potential increased to prevent excess electrons from escaping the plasma.[24] When both sources were powered and a positive voltage was applied to the substrate, the positive shift in the main ICP plasma potential caused a small extraction of electrons from the auxiliary ICP that apparently passed through the grounded metal mesh on top of the honeycomb-confining structure, leading to a small electron current to the substrate. When only the auxiliary source was on, a μA-level electron current was obtained, which increased with voltage. This could be stray electrons from the auxiliary ICP. The electron current was ~100 μA, corresponding to $\sim 6 \times 10^{14}$ electrons/s. Since the total substrate area was 3.0 cm^2 and assuming an electron velocity of the order of 10^7 cm/s, the electron density above the Si substrate was estimated to be of the order of 10^6 cm^{-3}. The main ICP density was around 1×10^{12} cm^{-3} (with 350 W input power), which indicated that the amount of electrons leaking from the auxiliary to the main ICP was negligible and should not affect the plasma operating condition. Likewise, a very small current of about −0.4 μA was recorded with a negative bias and was likely due to a low concentration of positive ions from the auxiliary ICP that passed through the honeycomb.

Possible communication or exchange between the two plasmas was also investigated by looking for changes in optical emission in the powered main ICP when the auxiliary ICP was turned on. Scattered light was collected through a viewport adjacent to a region downstream from the main ICP that contained the substrate support structure (see Fig. 1). Emission spectra from 730 to 920 nm were recorded for both sources on [Fig. 4(a)], the auxiliary ICP only [Fig. 4(b)], and the main ICP only (not shown). The intensity of light scattered from the main ICP was at least ~100 times higher than the intensity of light reaching this region from the distant auxiliary ICP. The spectrum in Fig. 4(c) was obtained by subtracting the spectrum recorded with just the main ICP on from that with both plasmas on. If the auxiliary ICP had no effect (positive or negative) on the main ICP, then the difference spectrum in Fig. 4(c) would be the same as the auxiliary spectrum in Fig. 4(b). The intensities of peaks in the difference spectrum in Fig. 4(c) are ~1% of that

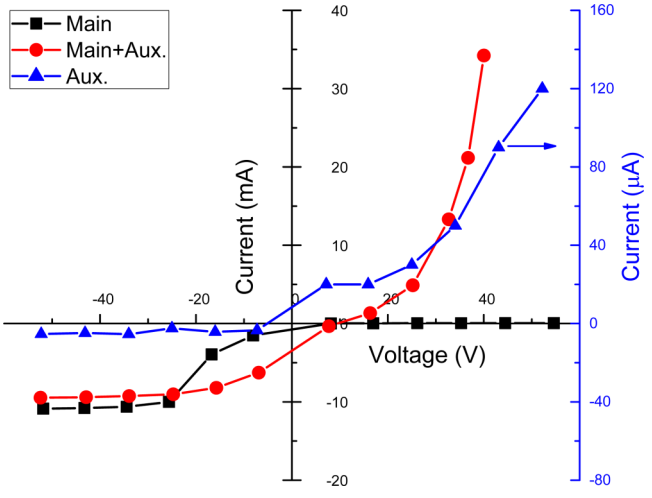

FIG. 3. Current through a Si substrate as a function of DC bias in the tandem system with 150 or 0 W auxiliary ICP power and 60 or 0 W main ICP power. The feed gas to the auxiliary ICP was 2.5 SCCM Ar/47.5 SCCM He and that to the main ICP was 10 SCCM Cl_2 and 240 SCCM Ar. The measured pressure in the main ICP was maintained at 60 mTorr. Note the different scales for depicting current.

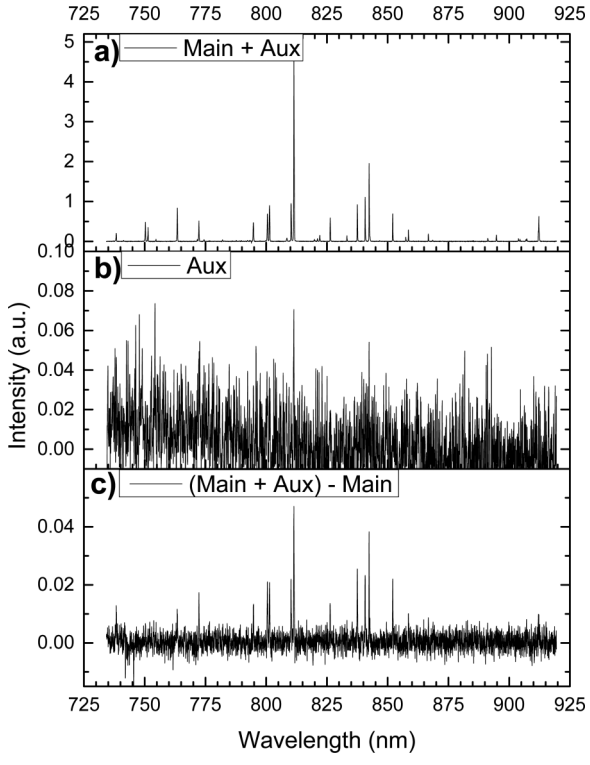

FIG. 4. Optical emission spectra (735–920 nm) recorded for (a) Main ICP + Auxiliary ICP, (b) Auxiliary ICP, and (c) (Main ICP + Auxiliary ICP) – Main ICP. The feed gas to the main ICP was 5 SCCM Cl_2 and 60 SCCM Ar mixture with 60 or 0 W plasma power, while the feed gas to the auxiliary ICP was 2.5 SCCM Ar and 47.5 SCCM He mixture with 200 W plasma power. The pressure in the main ICP was 15 mTorr.

05 September 2023 11:49:35

Published under an exclusive license by the AVS

recorded with just the main ICP on or both ICPs on [Fig. 4(a)] for the strong Ar and Cl features, such as the Ar 811.5 nm line, and undetectable (<0.5%) for the weaker 750.5 and 751.5 nm peaks. In fact, the intensities of ~0.05 and ~0.04 for the two most intense Ar lines at 811.5 and 842.5 nm in the difference spectrum are about equal to those peaks in the auxiliary ICP-only spectrum in Fig. 4(b). Even if some of the weaker lines that appear in Fig. 4(c) (e.g., 837.6 and 852.1 nm) are enhanced, the effect of the auxiliary ICP on the main ICP is at most 1%. Therefore, the optical emission measurements, together with the I-V characteristics of Fig. 3, indicate that the auxiliary ICP has no appreciable effect on the charge density, substrate ion flux, electron energy distribution, or Cl atom density of the main ICP, and that irradiation by VUV photons is the only reasonable explanation for the enhancements of up to 51% in etching rates (presented below) found with the addition of the auxiliary ICP VUV source.

B. Etching rates and surface morphologies

In the discussion below, PAE-only means that only the main plasma was on and the auxiliary plasma (VUV source) was off. PAE + VUV means that both main and auxiliary plasmas were on. In both cases, the sample was etched with the substrate electrode grounded, and the ion bombardment energy was below the ion-assisted threshold. Masked Si samples were etched for various times and then examined by SEM. Figure 5 shows cross-section SEM images as a function of etching time under PAE + VUV and PAE-only conditions. Except for the 2 s sputtering with RF power to the sample stage (−65 V DC self-bias) to remove the native oxide, the sample stage was grounded during etching. Similar etched feature shapes and surface morphologies were found for both PAE + VUV and PAE-only conditions. For relatively short etching times, the surfaces were smooth, while at longer times, pyramid features appeared (5 min etching time in Fig. 5). Since the ion energy in a Faraday-shielded ICP with a grounded sample stage is very low (i.e., ~5 eV), contaminants left after the brief RF bias cleaning step or formed during etching can act as micromasks.[4,25–30] Feature profiles consisted of sloped, flat sidewalls for samples etched for 2.5 and 5 min. A small, reentrant shape emerged at 10 and 20 min, along with a curvature in the sidewall and a more vertical average slope. Under no circumstances was significant undercutting observed at the SiO_2/Si interface. Similar sloped sidewalls were also observed in our previous studies.[3,4]

The substrate surface is a (100) plane, and the SiO_2 mask lines are aligned along a ⟨110⟩ direction. Therefore, the 125° ± 4° angle between the horizontal surface and the lower portion of the side wall in Fig. 5 (2.5, 5 and 10 min) is that expected for the (111) plane with respect to the (100) plane (125.3°). It has been reported that Cl atoms etch *n*-type Si (111) planes slower than (100) planes. Okano *et al.* reported an etching rate for Si(100) that was 30× higher than that of the (111) planes in a Cl_2 atmosphere with UV irradiation.[8] Ogryzlo *et al.* found that, regardless of the dopant, the etching rate of (111) *n*-type Si with atomic chlorine was about an order of magnitude smaller than that of (100) *n*-type Si.[31] They attributed this etching rate difference to the higher surface atom density of the (111) planes that caused steric hindrance on chemisorbed etchants (i.e., Cl atoms) leading to a slower penetration rate of Cl into the Si lattice. Matsuo *et al.* used XPS to study the Si surface after chlorine atom adsorption, where higher chlorides, $SiCl_2$ and $SiCl_3$, were found on both Si(100) and (111) surfaces, but the chlorinated layer on (111) was thinner than that on (100).[32] These higher chlorides desorbed after heating the surface to 300 °C. Their study suggests that the less-chlorinated surface of Si(111) would result in a slower etching rate. Crystallographic preference in etching rates is not observed in ion-assisted etching because energetic ion bombardment amorphizes the surface. In the present study, without energetic ion bombardment, the combination of Cl adsorption and VUV irradiation is less damaging; hence, crystal planes are preserved during etching, and slow etching of (111) planes persists as the (100) plane is etched to a depth of at least ~2 μm.

As shown in Fig. 6, the etched depths under either PAE + VUV or PAE-only conditions increase linearly as a function of etching time. The plasma conditions are the same as in Fig. 5. The etching rate was obtained from the slope of a linear least squares fit to the etched depth versus time measurements. The y-axis intercept corresponds to the Si removed by the 2 s RF bias step. From the slope of the fitted line, the etching rate is 169 ± 1 nm/min for PAE-only and 196 ± 1 nm/min for PAE + VUV conditions. Therefore, there is a significant 16 ± 1% enhancement in the etching rate in the presence of additional light from the auxiliary ICP.

It must be noted that when the main ICP was off, there was no detectable etching with only the VUV source (auxiliary ICP) on, regardless of whether the native oxide was removed by a 2 s etch with RF bias, or by a dilute HF solution.

The plasma power in the main ICP was reduced from 350 to 60 W, decreasing the photon flux and the Cl-atom density. The other conditions (gas flow rates and pressures in the auxiliary and main ICPs) were unchanged. SEM cross sections of etched samples are shown in Fig. 7. Relatively smooth surfaces were observed and small pyramid features were occasionally found, but generally such features were absent. The angle between the bottom surface and the side wall was 126° ± 1°, as was found at 350 W ICP power (Fig. 5).

The etched depths obtained from Fig. 7 are shown in Fig. 8. The etching rates derived from the slope of linear least squares fitted lines were 78.8 ± 1.0 and 87.7 ± 1.7 nm/min for PAE-only and PAE + VUV conditions, respectively. The etching rate enhancement when the VUV source was also turned on was 11 ± 3%. Compared with the etching rate in Fig. 6, while the main ICP power was reduced by a factor of ~6, the etching rate under PAE-only conditions decreased by only ~55%.

PAE-only etching rates as a function of power for several Cl_2 flow rates at a constant total (Cl_2 + Ar) flow rate and pressure are shown in Fig. 9, along with ion saturation currents for 10 SCCM Cl_2. Samples were sputtered for 2 s by applying RF power to the sample stage (which yielded −65 V DC self-bias) to remove the native oxide, before grounding the sample and etching under PAE-only conditions for 20 min. For a given Cl_2 flow rate, the etching rate increased with the plasma power, but with a diminishing slope, tending toward saturation at high power. On the other hand, the ion saturation current increased linearly with power.

At a high power density of ~0.21 W/cm^3 at 350 W, the ion saturation current to the sample is 62.4 mA, corresponding to an ion flux of 1.26×10^{17} cm^{-2} s^{-1}, which for an assumed T_e of 2 eV and Ar^+ as the dominant positive ion, yields an estimated plasma density of 1.0×10^{12} cm^{-3} at the sheath–presheath edge. At this

05 September 2023 11:49:35

Published under an exclusive license by the AVS

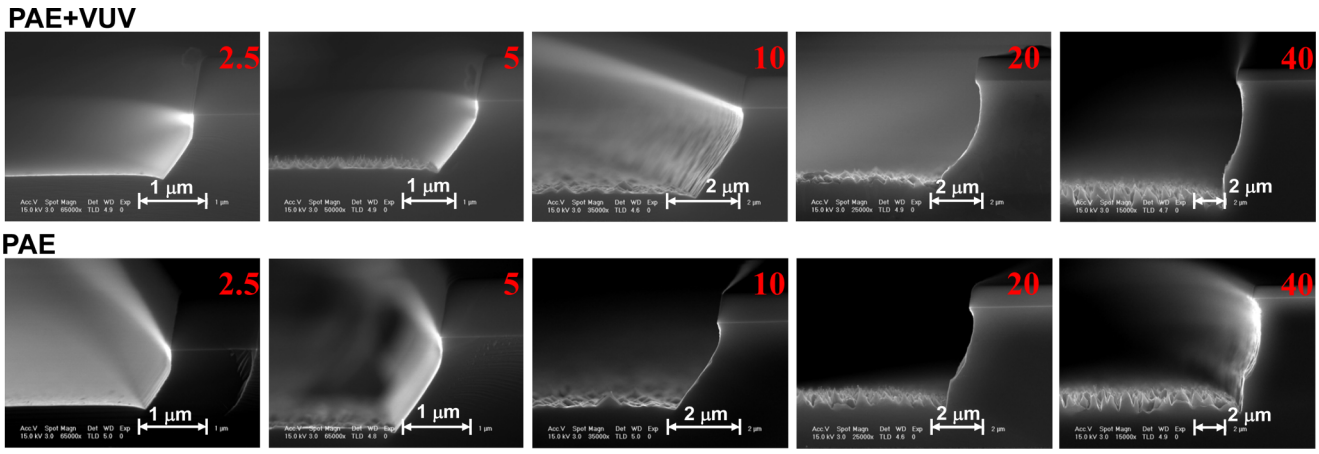

FIG. 5. Cross-sectional SEMs of patterned *p*-type Si etched with PAE + VUV (top row) and PAE only (bottom row) for different etching times (2.5, 5, 10, 20, and 40 min, left to right). The feed to the main ICP was 10 SCCM Cl_2 and 240 SCCM Ar (350 W power) and that to the auxiliary ICP was 2.5 SCCM Ar and 47.5 SCCM He (150 W power). The pressure in the main ICP was 60 mTorr.

high plasma density, nearly all of the Cl_2 in the main ICP is expected to be dissociated.[20,33,34] With 10 SCCM Cl_2 and 240 SCCM Ar, the maximum possible Cl-to-Ar number density ratio (n_{Cl}/n_{Ar}) corresponding to complete dissociation is, therefore, 0.083. At 60 mTorr, the estimated n_{Cl}/n_{Ar} from Eq. (3) with

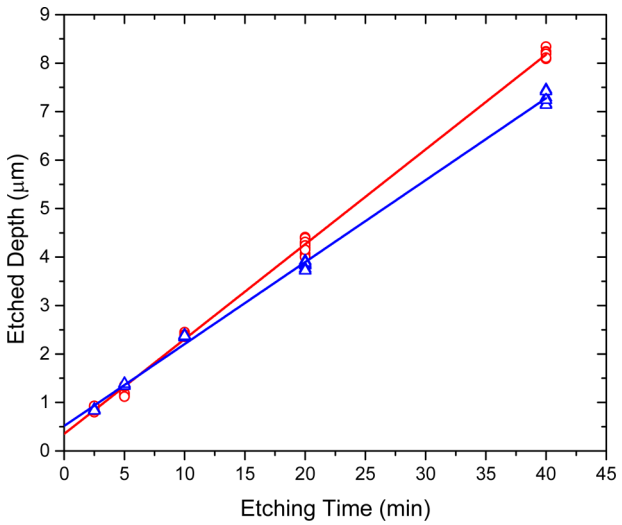

FIG. 6. Etched depth as a function of etching time for PAE-only (blue triangles) and PAE + VUV (red circles) conditions, determined from the SEM images in Fig. 5. The scattered points at a given time are measurements at several locations on the samples. The lines correspond to linear least squares fits to the measurements. The slopes of the fitted lines correspond to etching rates of 169 ± 1 nm/min for PAE-only and 196 ± 1 nm/min for PAE + VUV conditions. The respective y-intercepts of 0.514 ± 0.03 and 0.350 ± 0.02 μm indicate the amount of Si removed in the mask-patterning process, plus the 2 s oxide removal step with substrate bias.

$a_{Cl,Ar} \approx 1.2$ (estimated from an extrapolation of the lower pressure values given by Malyshev and Donnelly[34] and Ma *et al.*[21] to 60 mTorr) was about 0.086, consistent with nearly complete dissociation. With 5 SCCM Cl_2 and 245 SCCM Ar and 60 mTorr total pressure, when the main ICP power was reduced to 60 W, n_{Cl}/n_{Ar} estimated from actinometry was 0.034, compared with a maximum possible value of 0.041 for complete dissociation determined by the feed gas flow ratio. Since the gas temperature, T_g, will be somewhat higher at 350 W, compared with 60 W (Donnelly and Malyshev found that T_{gas} in a Cl_2 ICP increased ~twofold as power increased ~sevenfold),[35] and the Cl flux to the surface is proportional to $T_g^{-1/2}$, it is reasonable to assume that for each Cl_2 flow rate in Fig. 9, the Cl impingement rate is nearly independent of power.

With near-complete dissociation of Cl_2, the plasma is electropositive and $f_+ = 0.6 n_e u_B$ (where f_+ is the ion flux, n_e is the electron density in the bulk plasma, and u_B is the ion Bohm velocity). Therefore, the linear dependence of the ion flux on power indicates a linear increase in plasma density with power, a common feature of ICPs.[33,36,37] This is also expected to produce a VUV intensity that increases linearly with power. At a constant Cl_2 feed gas flow rate, the nearly constant Cl impingement and linearly increasing VUV flux as a function of power suggest that etching is increasingly starved for adsorbed Cl as power increases. The near linear increase in the etching rate with Cl_2 flow rate at constant power is also consistent with this conclusion.

A lower plasma pressure (15 mTorr) was also investigated with the minimum possible power (60 W) in the main ICP and a high power (200 W) in the auxiliary ICP. The main ICP flow rates were 60 SCCM Ar and 5 SCCM Cl_2, and the auxiliary ICP gas flows were 2.5 SCCM Ar and 47.5 SCCM He. Two patterned samples etched with PAE or PAE + VUV conditions are shown in Fig. 10. After 20- min etching, the average etched depth was about 1.38 μm for PAE only and 2.08 μm for PAE + VUV, corresponding to etching rates of 69 and 104 nm/min, respectively. Therefore, the added VUV flux from the auxiliary ICP caused a 51% enhancement in the

05 September 2023 11:49:35

Published under an exclusive license by the AVS

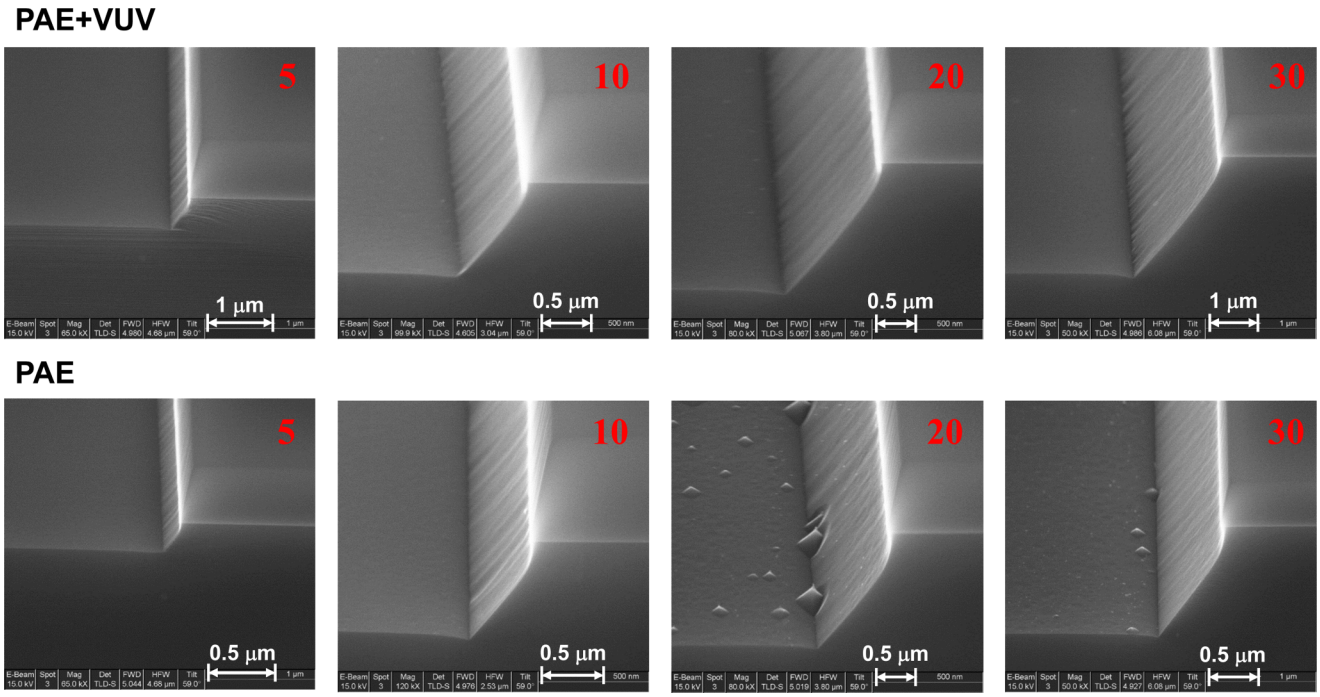

FIG. 7. Cross-sectional SEMs of patterned *p*-type Si etched with PAE + VUV (top row) and PAE only (bottom row) for different etching times (5, 10, 20, and 30 min, left to right). Plasma parameters were the same as in Fig. 5, except that the main ICP power was reduced to 60 W.

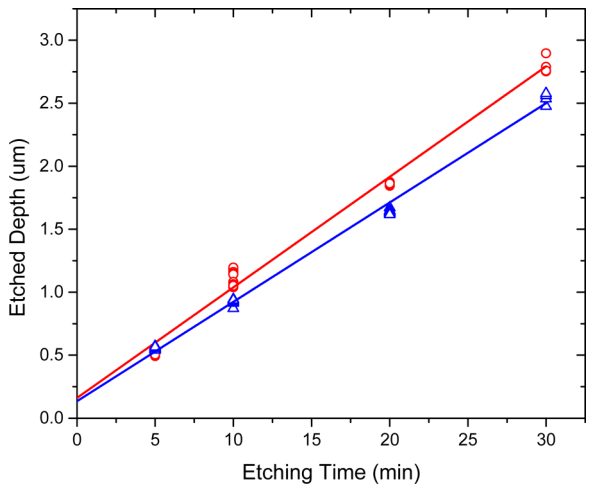

FIG. 8. Etched depth as a function of etching time for PAE-only (blue triangles) and PAE + VUV (red circles) conditions, determined from the SEM images in Fig. 7. The scattered points at a given time are measurements at several locations on the samples. The lines correspond to linear least squares fits to the measurements. The slopes of the fitted lines correspond to etching rates of 78.8 ± 1.0 nm/min for PAE-only and 87.7 ± 1.7 nm/min for PAE + VUV conditions. The respective y-intercepts of 0.135 ± 0.017 and 0.162 ± 0.030 μm indicate the amount of Si removed in the mask-patterning process, plus the 2 s oxide removal step with substrate bias.

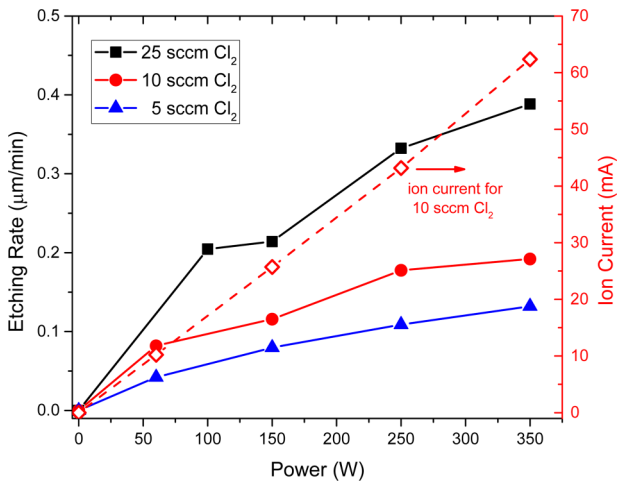

FIG. 9. Etching rate with only the main ICP on (PAE-only) as a function of power for different Cl_2 flow rates. The total flow rate of the Cl_2/Ar mixture was 250 SCCM and the pressure of the main ICP was kept at 60 mTorr. Ion saturation current was measured with a blank *p*-type Si sample with −65 V DC bias, a current collection area of 3.1 cm^2, and a Cl_2 flow rate of 10 SCCM.

05 September 2023 11:49:35

Published under an exclusive license by the AVS

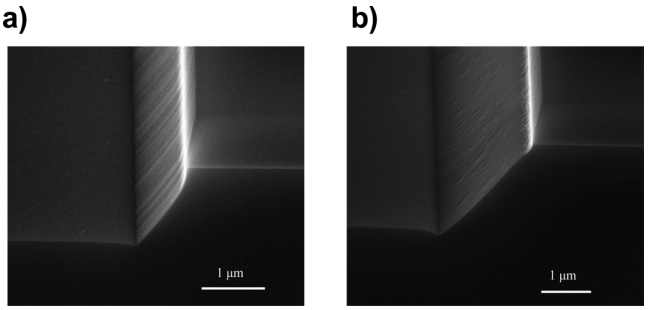

FIG. 10. Cross-sectional SEMs of patterned *p*-type Si etched with (a) PAE-only and (b) PAE + VUV for 20 min. Gas feed to the main ICP was 5 SCCM Cl_2 and 60 SCCM Ar mixture with 60 W power, while the VUV source (auxiliary ICP) feed gas was 2.5 SCCM Ar/47.5 SCCM He mixture with 200 W power. The pressure in the main ICP was 15 mTorr, and the estimated pressure in the VUV source ICP was 270 mTorr.

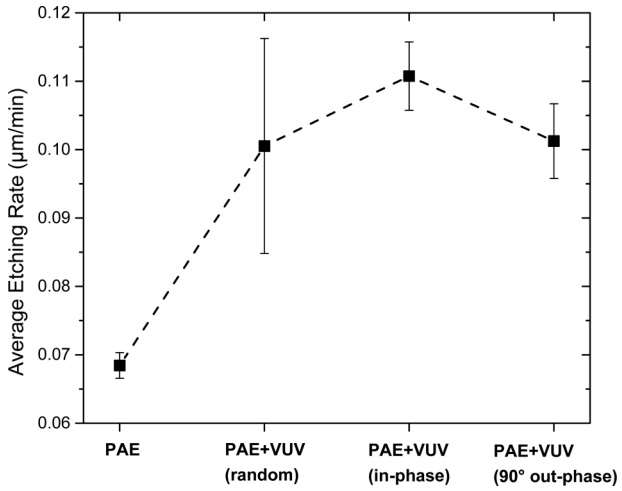

FIG. 11. Comparison of the average etching rate with different plasma phase conditions. Power to the auxiliary source was 200 W and that to the main ICP was 60 W. The feed to the main ICP was 5 SCCM Cl_2 and 60 SCCM Ar and that to the auxiliary ICP was 2.5 SCCM Ar and 47.5 SCCM He. The pressure in the main ICP was 15 mTorr, and the estimated pressure in the VUV source ICP was 270 mTorr.

etching rate for this set of conditions. The surfaces were relatively smooth after etching, and the same sloped sidewall feature was obtained, as in the higher-pressure experiments.

Lowering the plasma pressure from 60 to 15 mTorr causes T_e to increase, resulting in an increase in ion energy to the grounded sample. This raises the possibility of ion-assisted etching above the threshold energy of ~16 eV.[3,6,38,39] To evaluate this possibility, we estimated the maximum contribution by ion-assisted etching at 15 mTorr. Ion energy distributions were measured under similar plasma conditions in a previous study.[4,24] In a pure Ar inductively coupled plasma at 14 mTorr, about 5% of the ions strike the substrate with an energy greater than 16 eV. From the measured ion saturation current in the present study, the total impinging ion flux is about 1.9×10^{16} s^{-1} cm^{-2}; hence, the flux of ions with energies above 16 eV is ~8.8×10^{14} s^{-1} cm^{-2}.

Ion-assisted etching yields (Si atoms per incident ion) of <0.1 can be obtained by extrapolating measurements by Balooch *et al.* (Cl_2^+, or Cl_2 and Ar^+ beams) to 16 eV.[40] Similarly, Chang *et al.* reported a threshold of about 16 eV for etching of Si by beams of Cl and Ar^+.[39] An etching yield of <0.1 at 16 eV would result in a Si etching rate of <5×10^{15} Si/cm^2 min or <1 nm/min. The Si etching rate was 69 nm/min at 15 mTorr Ar at 60 W, and the contribution of ion-assisted etching is a negligible <1.4% at 15 mTorr and still less at 60 mTorr.

The 51% enhancement in the etching rate is attributed to a fourfold higher photon flux supplied by the auxiliary ICP (see Table I below). Some of the enhanced intensity is attributed to higher power (200 vs 150 W), but the main reason for the higher VUV photon flux from the auxiliary ICP onto the sample is a result of less absorption in the main ICP by Ar at 15 mTorr, compared with 60 mTorr.[16]

In all the experiments presented above, the main and auxiliary ICPs were powered independently. Consequently, the RF phase differences between the two sources were randomized over the course of an experiment. Since excitation of emission in plasmas is mainly caused by the electron impact and atomic radiative lifetimes are generally shorter than the RF period for frequencies below 20 MHz, emission intensities can be strongly modulated.[41–46] The radiative lifetimes of the Ar $1s_2$ and $1s_4$ states are 2.0 and 8.4 ns, respectively,[47,48] and the electron energy relaxation time was reported to be 16 ns under similar conditions[42]; hence, light from both sources might be expected to be modulated during the 37 ns period between peak positive and negative voltages at 13.56 MHz applied voltage frequency. Therefore, by syncing the phases of the two ICPs to be in-phase or 90° out-of-phase, the VUV flux from the auxiliary plasma will arrive at the substrate when the main ICP light flux is at a maximum or

05 September 2023 11:49:35

TABLE I. Summary of experimental conditions and measured etching rate with the corresponding photon flux and etching yield.

Aux. power (W)	Est. aux. press. (mTorr)	Aux Ar/He flows (SCCM)	Aux. photon flux (×10^{12} cm^2/s)	Main power (W)	Main press. (mTorr)	Main Cl_2/Ar flows (SCCM)	Main etch rate (nm/min)	Main plus aux. etch rate (nm/min)	PAE yield Si/photon	n_{Cl} (×10^{13} cm^{-3}) (@~T_{gas})
150	277	2.5/47.5	7.6	350	60	10/240	176	198	244	8.05 (600 K)
150	277	2.5/47.5	7.6	60	60	10/240	79	89	110	12.1 (400 K)
200	270	2.5/47.5	31.5	60	15	5/60	69	104	93	6.04 (400 K)

Published under an exclusive license by the AVS

minimum intensity, respectively, while maintaining a constant Cl atom flux. Since the etching rate approaches saturation at higher power and, hence, VUV flux (Fig. 9), the enhancement in the etching rate from the auxiliary ICP light when 90° out-of-phase with the main ICP may be expected to be larger than when the two ICPs are powered in-phase. Conversely, if the VUV intensity causes a flattening of the bands at the surface (see discussion below), then the effect of the added VUV flux may be lessened if the two ICPs are 90° out of phase.

To investigate this, the two function generators supplying power to the two ICPs were synchronized, with phase differences of 0° or 90°. Figure 11 presents etching rates obtained with just the main ICP, and with the main and auxiliary ICPs powered in-phase, 90° out-of-phase, and with random phase (i.e., no syncing between the two function generators). All samples were etched for 20 min. The etching rates for all three dual ICP experiments were significantly larger (by ~30%) than when just the main ICP was on. While the in-phase etching rate was about 10% larger than the 90° out-of-phase value, within the uncertainty of the measurement, it is not statistically higher than either the 0° or random phase measurement. Perhaps this result is not surprising, given that radiation trapping and production of emission from low-energy electron collisions with the metastable states will likely lengthen the emission lifetimes beyond the RF half-period.[14]

C. Surface chemistry

After etching, Si samples were transferred under vacuum to the XPS chamber for surface analysis. Figure 12 shows XPS low-resolution spectra under a typical plasma condition for either PAE-only or PAE + VUV conditions. The samples were otherwise grounded during etching. Major peaks include Si 2p (99.6 eV), Si 2 s (150.9 eV), Cl 2p (200.4 eV), and Cl 2 s (271.8 eV). No impurities (e.g., O, C, or metals) were detected. The relative chlorine surface concentrations ([Cl]/[Si]) were 0.156, 0.166, 0.154, and 0.152 for PAE + VUV RF-sputter cleaned, PAE + VUV HF-cleaned, PAE-only RF-sputtered, and PAE-only HF-cleaned, respectively. The low relative chlorine surface concentration, in the absence of energetic ion bombardment, is consistent with our previous finding that, under PAE conditions, the surface contains only SiCl.[6] Similar results have been reported by Bogart and Donnelly, where the sidewall surface of masked features had 50% less Cl than the ion-bombarded bottom surface.[49] The finding that the combination of the main ICP and the VUV source resulted in the same surface [Cl]/[Si] ratio as that with the main ICP alone implies that the surface chemistry during etching had changed little by the extra VUV photon flux.

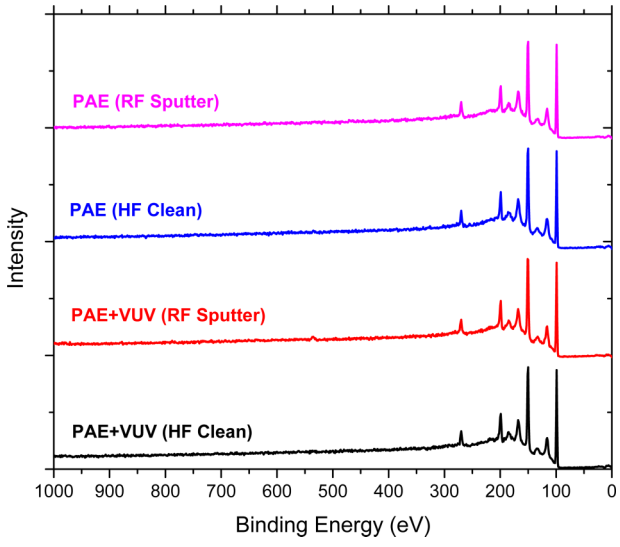

FIG. 12. Low-resolution XPS survey spectra (takeoff angle of 30°) of *p*-type Si after etching for 20 min. HF Clean: 60 s dip in 2% HF solution. RF sputter: 2 s of *in situ* RF sputtering. The feed gas of the main ICP (350 W power) was 10 SCCM Cl_2 and 240 SCCM Ar and that of auxiliary ICP (150 W power) was 2.5 SCCM Ar and 47.5 SCCM He. The pressure in the main ICP was 60 mTorr, and the estimated pressure in the VUV source ICP was 277 mTorr.

D. Photo-assisted etching yields

The PAE yield was determined by dividing the measured etching rate enhancement (additional Si atoms/cm^2 s resulting from the auxiliary ICP light) by the measured VUV photon flux to the sample surface from the auxiliary source. The photon flux was obtained by measuring the photoemission current through a gold thin film on a copper disk placed at the position of the Si sample in the main chamber. Negative DC bias was applied to the substrate, and the VUV-produced photoelectrons were repelled toward a stainless steel electron collector that surrounded the Au/Cu detector. Details of this measurement can be found in another publication.[16] In those measurements, Ar was present in the downstream chamber to mimic the self-absorption and back diffusion (main-to-auxiliary ICP) during etching. The main ICP was not powered, however, and no Cl_2 was present. With the main ICP powered, most of the Cl_2 was dissociated, and besides, the absorption coefficient of Cl_2 near 105 nm was too small to significantly attenuate the light from the auxiliary ICP.[50] Cl atoms will not absorb Ar emission from the auxiliary ICP.

PAE yields for three cases are summarized in Table I. Remarkably high yields of about ~90 to ~240 Si atoms per VUV photon were obtained from this analysis. These high yields are also consistent with the revised value of ~80 by Shin *et al.*[3] (see discussion in the Introduction section) and are almost equal to those reported by Schwentner and co-workers[12,51] at similar VUV wavelengths for Si etching in the presence of XeF_2 and GaAs etching in the presence of Cl_2. Given the rather small enhancement in the VUV flux provided by the auxiliary ICP in most of the cases, as shown in Table I, combined with other uncertainties, it is hard to draw additional conclusions from the range of PAE yields for different conditions.

E. Etching mechanism

It was shown above that VUV photons induce etching of *p*-type Si by a chlorine- containing plasma and that the etching rate can be enhanced by additional VUV photons generated by a tandem auxiliary ICP. No etching occurs with only auxiliary VUV

05 September 2023 11:49:35

Published under an exclusive license by the AVS

irradiation in the presence of just Cl_2 (i.e., with the main ICP power off). The inability of Cl_2 gas alone to etch *p*-type or semi-insulating Si at room temperature was observed by many researchers. Etching can occur in a Cl_2 atmosphere with simultaneous exposure of the Cl_2 gas above the surface and the Si surface to UV light.[8,11] The gas-phase irradiation results in the photodissociation of Cl_2 and the generation of Cl atoms. Compared with these studies, the VUV source used in the present work had a much lower photon flux. Thus, with the main ICP plasma off, any photon-induced Cl_2 dissociation to form Cl that could lead to etching of the VUV-irradiated Si substrate was insignificant. Therefore, no etching was observed with the VUV source only, and the main plasma was required to generate Cl atoms that are needed for photo-assisted etching of *p*-type Si.

The etching rates for the main ICP summarized in Table I of 176, 79, and 69 nm/min for the estimated corresponding Cl partial pressures of 5, 5, and 1.25 mTorr correspond to the etching rates of 35.2, 15.8, and 55.2 nm/(min mTorr). These values are roughly 100 times faster than those reported by Walker and Ogryzlo[52] for the etching of semi-insulating polycrystalline Si by Cl atoms in the absence of a plasma or light and perhaps 1000 times faster than the etching of *p*-type Si.[8] The fast etching rates in the present study are comparable to only those reported for heavily doped (10^{19}–10^{20} cm^{-3}) *n*-type Si [polycrystalline[52] and (100) single crystal[31]]. The question then arises: Could relatively low levels of VUV light create conditions on the surface of *p*-type Si that would be similar to those of heavily doped *n*-type?

Several mechanisms have been proposed for the enhancement of the etching rate of *n*-type Si by F and Cl atoms. Winters and Haarer[53] studied the etching of Si by XeF_2 gas (no plasma) and attributed the etching behavior as a function of dopant type and concentration to the formation of F^- on the surface, invoking a mechanism analogous to that proposed by Cabrera and Mott[54] to explain the oxidation of Si. Although not the subject of that study, Winters and Haarer proposed that a similar mechanism may be responsible for the more dramatic dopant dependence in the etching of Si by Cl atoms.

Such effects are often explained with the aid of energy band diagrams of the near surface region, such as those in Fig. 13. E_V and E_C are the energies at the edges of the valence and conduction bands, E_i is the intrinsic energy level (i.e., close to midway between the bandgap energy, $E_g = 1.12$ eV), E_F is the Fermi energy level, and V_p is the plasma potential. The Si work function, electron affinity level, and vacuum energy level are indicated by the symbols ϕ, ψ, and E_{VAC}, respectively. A^- and D^+ represent the immobile acceptor and donor ions, respectively. At the surface, the conduction and valence bands can move up or down with respect to the Fermi level energy due to a variety of possible surface defects that tend to pin the surface Fermi level near the midgap intrinsic energy level. This leads to downward-bending conduction and valence bands in *p*-type semiconductors and upward-bending bands in the *n*-type material. Surface band bending has been widely reported for Si; the results vary widely with surface treatments and dopant type and concentration. Arita *et al.*[55] found that little band bending occurred for HF-passivated Si(100) until the dopant level (both *p*- and *n*-type) exceeded 10^{15} cm^{-3}, whereupon further increases in dopant concentrations, approaching the density of states of the valence band maximum and conduction band minimum, led to a downward and upward band bending of about 0.5 eV or about half the bandgap energy of 1.12 eV, i.e., the Fermi level was pinned near mid bandgap for both *p*-type and *n*-type Si.

What is more relevant in the present case, however, is the degree of band bending when the moderately doped *p*-type Si(100) is exposed to a chlorine plasma. Unfortunately, such measurements or calculations have not been reported thus far. Vaquila *et al.* measured the degree of band bending for a clean Si(100) 2×1.[56] For *p*-type and *n*-type doping levels of $\sim 10^{18}$–10^{19} cm^{-3}, they found that the E_F was 0.24 eV below E_i at the surface in both cases.[56] Kim *et al.* treated *n*-type $Si_{0.83}Ge_{0.17}$ (1×10^{17} cm^{-3} phosphorus-doped) with an Ar or N_2 ICP and found that at the surface, E_C–E_F = 0.53 eV, i.e., near the middle of the bandgap.[57]

Perhaps more relevant are studies of cleaved (110) surfaces of GaAs and InP after exposure to Cl_2. Clean (110) planes of these materials are relatively free of surface states, and, thus, the surface Fermi level energy is nearly equal to that of the bulk crystal. Troost *et al.* found that when a GaAs (110) surface was exposed to small doses of Cl_2, the surface Fermi level for 3×10^{16} cm^{-3} *p*-type moved only slightly toward the E_V, while for 1.3×10^{17} cm^{-3} *n*-type, E_F dropped by about 1 eV to a value 0.2 eV above E_V.[58] At larger doses of Cl_2, the surface E_F of both types shifted to 0.55 eV above E_V. Similar, though less dramatic, effects were found by Mönch for InP (110).[59]

The above studies taken as a whole suggest that E_F for *n*-type Si exposed to a chlorine plasma would be pinned near mid bandgap and, though less certain, would also suggest this to be the case for *p*-type Si. With these assumptions, the qualitative energy band diagrams in Fig. 13 describe the near-surface region of *p*-type and *n*-type Si for a chlorinated surface in the absence of a plasma and for *p*-type Si in the presence of a plasma. The Si substrate is grounded. Far from the surface, the Fermi energy with respect to the valence band maximum is given by

$$E_F - E_V = kTln\left[\frac{N_V}{N_A}\right], \tag{5}$$

where k is the Boltzmann constant, T is the substrate temperature in K (assumed to be 300 K), N_V is the density of states at the valence band maximum (1.8×10^{19} cm^{-3}), and N_A is the acceptor concentration, which equals the hole concentration n_p for fully electrically activated dopants. For the experiments described in this study, n_p varies between 1×10^{14} and 4×10^{15} cm^{-3}. Hence, E_F–E_V far from the surface is between 0.31 and 0.22 eV.

The presence of negative halogen ions (F^- and Cl^-) on the surface and/or the near surface region has been widely invoked to explain the aspects of Si etching in fluorine- and chlorine-containing plasmas, including the dependence of the etching rate on dopant number density and type.[60,61] It has been argued that the formation of F^- and Cl^- is energetically favorable because their electron affinity levels in Si lie below the valence band edge of Si.[53]

As shown in previous XPS measurements,[6] without energetic ion bombardment (grounded substrate), the surface layer consisted only of Si and SiCl. Furthermore, the Si:Cl atomic ratio in the layer measured by the Si(2p)-to-Cl(2p) intensity ratio was within

05 September 2023 11:49:35

Published under an exclusive license by the AVS

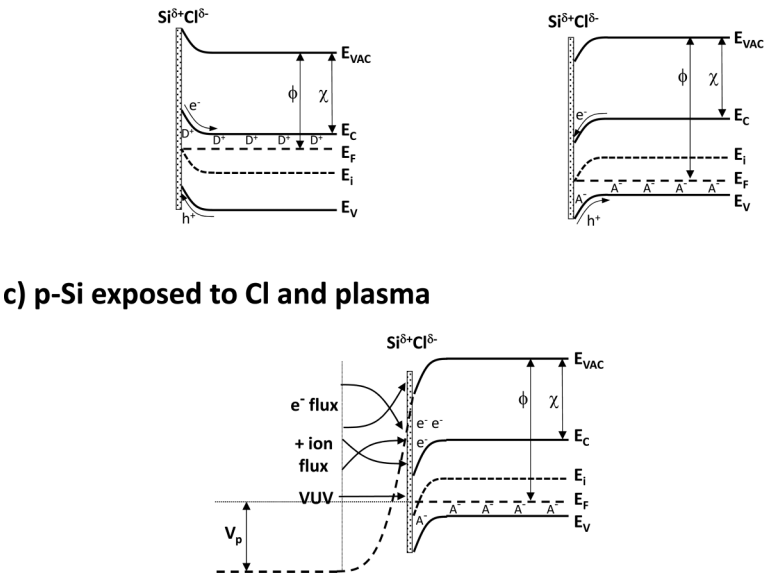

FIG. 13. Qualitative band diagram near the surface of chlorine-exposed *n*-type and *p*-type Si in the absence of a plasma and for *p*-type Si in the presence of a plasma.

experimental uncertainty (<5%) equal to the Si:Cl ratio computed from a deconvolution of the Si(2p) high-resolution spectrum. This indicates that any additional "free" chlorine in the layer is much less than the amount of Cl bound to Si or that some more weakly bound chlorine desorbs between plasma exposure and XPS analysis. The latter possibility was previously discounted in studies employing *in situ*, real-time laser-induced desorption[62] and ellipsometry,[63] where phenomena related to surface layer composition and thickness (SiCl desorbed by the laser[62] and the ellipsometric quantities ψ and Δ[63]) remained unchanged after the plasma and substrate bias were simultaneously extinguished. Consequently, Cl^-, a possible reactive intermediate in etching, is likely present in the surface layer in amounts much less than a monolayer during plasma exposure. Although the Si–Cl bond is partially ionic, the partial negative charge on Cl is equal to the partial positive Si charge; hence, only additional Cl^- can add a negative charge to the surface region.

The Cl_2/Ar ICP can have additional effects on surface band bending due to the electric field imposed by the plasma sheath as well as positive ion and electron impingement. At the estimated plasma density of 1.0×10^{12} cm^{-3} at the sheath–presheath edge, the Debye length is 10 μm. The (Child law) sheath width is

$$s = \frac{\sqrt{2}}{3}\left(\frac{2V_s}{T_e}\right)^{0.75}\lambda_D. \quad (6)$$

Hence, assuming a sheath potential of about $V_s = 10$ V, $s \approx 25\,\mu$m.

The voltage between the plasma and the surface potential (here, the back of the sample is at ground potential) is divided between the plasma sheath, the chlorinated surface layer, and the Si substrate. The voltage drop across the bulk substrate can be ignored (for the 5–100 Ω cm resistivity, its resistance is between ~0.1 and 2 Ω). We can further ignore the small voltage (<0.3 V) across a Schottky barrier at the contact between the scratched back of the Si substrate and the melted indium contact that is placed on the grounded sample holder.

The electrical description of the plasma–semiconductor interface resembles that of the metal-oxide-semiconductor diode, where the "metal" is the bulk plasma, the "oxide" is the plasma sheath, and the semiconductor is the silicon substrate, with the chlorinated Si near-surface region corresponding to the interface trapped charge. This interface region would be ~1 -nm thick.

Assuming that the entire voltage drop is between the plasma potential and the grounded sample, the electric field at the Si surface is ~4 kV/cm. This is not large enough to cause much of an effect on band bending. Besides, as pointed out by Tchertchian *et al.*,[64] the voltage across the plasma sheath will only add to the degree of the downward bending of bands at the surface of a *p*-doped semiconductor, as depicted in Fig. 13(c), presumably having no effect, or even slowing the etching rate by Cl atoms.

When a 104 -nm (11.92 eV) photon is absorbed by Si, the electron–hole (e–h) pair created possesses a total energy of 11.92–1.12 = 10.8 eV. This energy is quickly dissipated mainly by creating about three additional e–h pairs.[65–67] Therefore, yields for carrier-driven etching by photons with this energy could be perhaps four times that for lower energy UV photons with a comparable penetration length and reflectivity. When a positive ion such as Ar^+ approaches very close to a Si surface (i.e., a couple Å), an electron from Si below the surface leaves the valence band and tunnels through the vacuum to neutralize the ion, leaving a hole in the valence band.[68] To conserve energy, a second (Auger) electron is promoted from the valence band to

05 September 2023 11:49:35

Published under an exclusive license by the AVS

the conduction band. The excess energy from the ion neutralization process is $E_{IP} - q\phi_S$, where E_{IP} is the Ar ionization potential at a short distance from the surface and ϕ_S is the work function. If E_{IP} does not differ much from the ionization energy of the isolated atom, then ~10.9 eV is the initial excess energy left from the ion neutralization. This energy is then distributed between the Auger electron and the two holes created in the overall process. It has been found that very few of the Auger electrons escape into the vacuum (<0.5%).[68] An electron either from the sample in contact with ground or from the plasma for electrically floating samples balances the excess positive charge left by positive ion neutralization, so at least two electron–hole pairs are created per Ar^+ neutralized at the surface. The excess energy of the energetic Auger electron and two holes likely leads to the creation of an additional e–h pair. Consequently, positive ion neutralization at the surface produces nearly the same result as the absorption of a VUV photon.

Since the positive ion flux is about 10 000 times larger than the photon flux produced by the auxiliary ICP (VUV source), if etching is governed by e–h production, then the auxiliary photons should produce an ~0.01% increase in the rate of etching caused by the carriers generated by the flux of low energy ions, contrary to the 10%–50% enhancement. This seemingly rules out VUV photon-generation of carriers as the mechanism.

Additionally, it is likely that the low-energy ion flux is of the order of 100 times larger than the majority of the impinging photon flux, generated in the main ICP. It has been shown (Fig. 8 of a previous publication from this laboratory[3]) that when the flux of low energy ions was blocked, while allowing Cl atoms and VUV photons to reach the surface, the substantial etching rate of *p*-type Si did not change. This, therefore, indicates that the electrons and holes created in the ion neutralization process do not play a role in etching. Consequently, neither can carriers generated by VUV photons.

This seemingly leaves only a photochemical process as the cause of etching by these energetic photons. Since the yields greatly exceed unity, the process must be catalytic in nature. There have been reports of photocatalytic processes with yields greatly exceeding one per photon. For example, Whetten *et al.* reported that with a pulsed N_2 laser light of 337 nm, the quantum yields reached as high as 408 and 18 for gas-phase photocatalytic isomerization and hydrogenation of 1-pentene, respectively, by gaseous iron penta-carbonyl.[69] Yanagida *et al.* reported quantum yields as high as 13 for *cis-trans* isomerization of alkenes on ZnS and CdS.[70]

The role of a catalyst is to reduce an energy barrier or barriers that allow an exothermic reaction or a series of reactions to occur. For Cl atom etching of Si, the following overall reactions (with corresponding heats of reaction[71]) can be written:

$$Si_{(s)} + Cl_{(g)} \rightarrow SiCl_{(g)} \qquad \Delta H = 77 \text{ kJ/mol}, \qquad (7)$$

$$Si_{(s)} + 2Cl_{(g)} \rightarrow SiCl_{2(g)} \qquad \Delta H = -411 \text{ kJ/mol}, \qquad (8)$$

$$Si_{(s)} + 3Cl_{(g)} \rightarrow SiCl_{3(g)} \qquad \Delta H = -754 \text{ kJ/mol}, \qquad (9)$$

$$Si_{(s)} + 4Cl_{(g)} \rightarrow SiCl_{4(g)} \qquad \Delta H = -1147 \text{ kJ/mol}. \qquad (10)$$

Hence, only etching of Si by Cl to produce SiCl [reaction (7)] is endothermic.

Chemisorption of Cl and desorption of reaction products stimulated by VUV photons (or for *n*-type Si, occurring spontaneously) are unlikely to occur in a concerted process. Consequently, some if not most of the energy released in Cl chemisorption is unavailable to aid product desorption. Since the surface is covered with mostly SiCl, it is the precursor to etching. The photodesorption of SiCl is one possible process, but this generates a single etching product and a Si surface dangling bond site, per absorbed photon, and does not likely initiate a chain reaction.

If on the other hand, the photon-stimulated desorption process leads to the creation of positive and negative ion pairs, chain reactions could follow. One scenario is depicted in Fig. 14. The absorption of a VUV photon leads to the breaking of a R-Si bond, such that R^- forms and desorbs, and the Si atom left behind possesses a + charge. R can be Cl or SiCl, or perhaps even $SiCl_2$ or $SiCl_3$, though the absence of these species in XPS spectra make this less likely. Electron transfer from an adjacent SiCl–Si bond to the positively charged Si could weaken the bond between SiCl and the Si surface. Cl transfer from an adjacent SiCl could lead to a prompt desorption of $SiCl_2$ and a + charge on the electron-donating Si surface atom. This process could continue many times as patches of the SiCl-covered Si surface are converted to Si dangling bond sites that will subsequently chemisorb Cl generated by the plasma. An electron from either the plasma or the bulk would terminate the chain reaction by neutralizing the Si^+ surface catalyst. There are, of course, other possible reaction pathways.

It should be noted that the generation of a positive charge at the surface by photostimulated desorption of a negative ion would be equivalent to the migration of holes to the surface of *n*-type Si that is expected due to the pinning of the Fermi level near mid-bandgap. In this sense, VUV photons absorbed at the surface of *p*-type Si may play the same role as minority carries in *n*-type Si in promoting etching by Cl.

While photon-stimulated desorption of neutrals has been more thoroughly investigated, the desorption of negative ions has also been reported. Such ion pair formation or "dipolar desorption" processes leave behind a positive surface charge.[72,73] Wen and Chou have observed that when CF_3Cl is adsorbed on Si(111)-7 × 7 at 30 K, F^- desorbs when irradiated by photons with energies of 12–35 eV.[72] Four maxima in F^- desorption intensity were observed over this range of energy. The photodesorption spectrum is very different from the photodissociation process in the gas phase, which also results in ion pair formation. This disparity and the high photodesorption yields were attributed to the role of electron attachment of the positive ion product on the surface. Siller *et al.* have studied photodesorption following the adsorption of O_2 and CO on graphite.[74] In both cases, they observe O^- as the product, with very little positive ion desorption.

Confirmation of such a photocatalytic chain reaction, initiated by negative ion photodesorption, will require further experiments and more advanced theories.

05 September 2023 11:49:35

Published under an exclusive license by the AVS

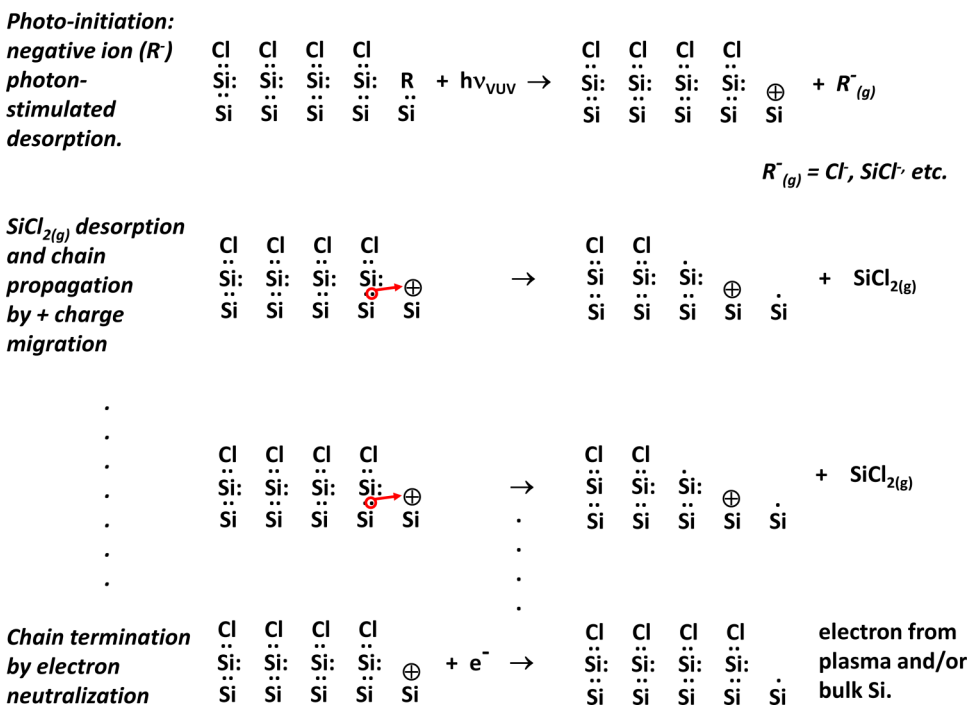

FIG. 14. One possible mechanism for photocatalytic etching of Si by Cl, initiated by negative ion photodesorption.

IV. SUMMARY AND CONCLUSIONS

The influence of additional VUV irradiation on the in-plasma PAE of *p*-type Si was investigated. The main ICP (using Cl_2/Ar gas) was in tandem with an auxiliary ICP (acting as a VUV source) in Ar/He gas. The two ICPs were separated by a grounded tungsten grid and a bundle of high-aspect-ratio quartz tubes that blocked charged species but allowed photons from the auxiliary plasma to reach the substrate in the main plasma, providing an independent and controllable VUV photon flux. The etched profiles and surface morphology of the masked samples were studied by SEM, while the surface composition of blanket Si samples was analyzed by XPS. A moderate ~10% enhancement of etching rate was observed by adding an extra VUV photon flux (PAE + VUV) under different plasma conditions at 60 mTorr and from 60 to 350 W in the main ICP. The maximum enhancement was 51% at the minimum possible power in the main ICP and maximum possible VUV light generated by the auxiliary ICP. The XPS analysis showed that the degree of chlorination of the Si surface was identical for PAE-only and PAE + VUV conditions, consisting of SiCl with little if any higher chlorides.

Based on the *in situ*–measured extra photon flux to the substrate, reported elsewhere, the PAE yield was estimated to be incredibly high, ranging from 90 to 240 Si/photon. Several arguments were made to rule out the generation of electron–hole pairs as the likely mechanism for the large PAE yields. Instead, VUV photons were more likely causing a photocatalytic chain reaction. A possible mechanism was proposed in which photostimulated desorption of a negative ion leaves behind a positive charge on the Si surface that weakens the bond between SiCl and the surface leading to the desorption of $SiCl_2$.

ACKNOWLEDGMENTS

This work was supported financially by the National Science Foundation (NSF) (No. PHY-1500518) and the Department of Energy, Office of Fusion Energy Science (No. DE–SC0001939).

AUTHOR DECLARATIONS

Conflict of Interest

The authors have no conflicts to disclose.

DATA AVAILABILITY

The data that support the findings of this study are available within the article.

REFERENCES

[1]V. M. Donnelly and A. Kornblit, J. Vac. Sci. Technol. A **31**, 050825 (2013).
[2]K. J. Kanarik, T. Lill, E. A. Hudson, S. Sriraman, S. Tan, J. Marks, V. Vahedi, and R. A. Gottscho, J. Vac. Sci. Technol. A **33**, 020802 (2015).
[3]H. Shin, W. Zhu, V. M. Donnelly, and D. J. Economou, J. Vac. Sci. Technol. A **30**, 021306 (2012).
[4]W. Zhu, S. Sridhar, L. Liu, E. Hernandez, V. M. Donnelly, and D. J. Economou, J. Appl. Phys. **115**, 203303 (2014).
[5]S. Sridhar, L. Liu, E. W. Hirsch, V. M. Donnelly, and D. J. Economou, J. Vac. Sci. Technol. A **34**, 061303 (2016).
[6]E. W. Hirsch, L. Du, D. J. Economou, and V. M. Donnelly, J. Vac. Sci. Technol. A **38**, 023009 (2020).
[7]L. Du, E. W. Hirsch, D. J. Economou, and V. M. Donnelly, J. Vac. Sci. Technol. A **38**, 053003 (2020).
[8]H. Okano, Y. Horiike, and M. Sekine, Jpn. J. Appl. Phys. **24**, 68 (1985).

05 September 2023 11:49:35

Published under an exclusive license by the AVS

[9]R. Kullmer and D. Bauerle, Appl. Phys. A: Solids Surf. **47**, 377 (1988).
[10]W. Sesselmann, E. Hudeczek, and F. Bachmann, J. Vac. Sci. Technol. B **7**, 1284 (1989).
[11]R. B. Jackman, H. Ebert, and J. S. Foord, Surf. Sci. **176**, 183 (1986).
[12]V. Ney and N. Schwentner, J. Phys.: Condens. Matter **18**, S1603 (2006).
[13]U. Streller, B. Li, A. Krabbe, H. P. Krause, I. Twesten, and N. Schwentner, J. Electron Spectrosc. Relat. Phenom. **80**, 49 (1996).
[14]P. Tian and M. J. Kushner, Plasma Sources Sci. Technol. **26**, 024005 (2017).
[15]B. Li, U. Streller, H-P Krause, I. Twesten, and N. Schwentner, J. Appl. Phys. **77**, 350 (1995).
[16]L. Du, P. Ruchhoeft, D. J. Economou, and V. M. Donnelly, J. Vac. Sci. Technol. B **40**, 022206 (2022).
[17]N. Layadi, V. M. Donnelly, and J. T. C. Lee, J. Appl. Phys. **81**, 6738 (1997).
[18]F. Hutchinson, J. Chem. Phys. **17**, 1081 (1949).
[19]F. Sharipov and V. J. Benites, J. Chem. Phys. **143**, 154104 (2015).
[20]N. L. Bassett and D. J. Economou, J. Appl. Phys. **75**, 1931 (1994).
[21]T. Ma, T. List, and V. M. Donnelly, J. Vac. Sci. Technol. A **35**, 031303 (2017).
[22]T. Ma, T. List, P. Arora, and V. M. Donnelly, J. Appl. Phys. **125**, 023301 (2019).
[23]E. Karakas, V. M. Donnelly, and D. J. Economou, Appl. Phys. Lett. **102**, 034107 (2013).
[24]H. Shin, W. Zhu, L. Xu, V. M. Donnelly, and D. J. Economou, Plasma Sources Sci. Technol. **20**, 055001 (2011).
[25]G. S. Oehrlein, J. Vac. Sci. Technol. B **8**, 1199 (1990).
[26]H. Tsuda, N. Nakazaki, Y. Takao, K. Eriguchi, and K. Ono, J. Vac. Sci. Technol. B **32**, 031212 (2014).
[27]H. Nabesawa, T. Hitobo, S. Wakabayashi, T. Asaji, T. Abe, and M. Seki, Sens. Actuators B **132**, 637 (2008).
[28]I. I. Amirov and A. S. Shumilov, High Energy Chem. **42**, 399 (2008).
[29]E. Gogolides, C. Boukouras, G. Kokkoris, O. Brani, A. Tserepi, and V. Constantoudis, Microelectron. Eng. **73-74**, 312 (2004).
[30]M. Martin and G. Cunge, J. Vac. Sci. Technol. B **26**, 1281 (2008).
[31]E. A. Ogryzlo, D. E. Ibbotson, D. L. Flamm, and J. A. Mucha, J. Appl. Phys. **67**, 3115 (1990).
[32]J. Matsuo, K. Karahashi, A. Sato, and S. Hijiya, Jpn. J. Appl. Phys. **31**, 2025 (1992).
[33]N. C. M. Fuller, I. P. Herman, and V. M. Donnelly, J. Appl. Phys. **90**, 3182 (2001).
[34]M. V. Malyshev and V. M. Donnelly, J. Appl. Phys. **88**, 6207 (2000).
[35]V. M. Donnelly and M. V. Malyshev, Appl. Phys. Lett. **77**, 2467 (2000).
[36]Y. J. Lee, K. N. Kim, B. K. Song, and G. Y. Yeom, Thin Solid Films **435**, 275 (2003).
[37]R. J. Hoekstra and M. J. Kushner, J. Appl. Phys. **79**, 2275 (1996).
[38]J. P. Chang and H. H. Sawin, J. Vac. Sci. Technol. B **19**, 1319 (2001).
[39]J. P. Chang, J. C. Arnold, G. C. H. Zau, H.-S. Shin, and H. H. Sawin, J. Vac. Sci. Technol. A **15**, 1853 (1997).
[40]M. Balooch, M. Moalem, W-.E. Wang, and A. V. Hamza, J. Vac. Sci. Technol. A **14**, 229 (1996).
[41]V. M. Donnelly, D. L. Flamm, and R. H. Bruce, J. Appl. Phys. **58**, 2135 (1985).
[42]D. L. Flamm and V. M. Donnelly, J. Appl. Phys. **59**, 1052 (1986).
[43]D. B. Graves, J. Appl. Phys. **62**, 88 (1987).
[44]F. Tochikubo, A. Suzuki, S. Kakuta, Y. Terazono, and T. Makabe, J. Appl. Phys. **68**, 5532 (1990).
[45]T. Kokubo, F. Tochikubo, and T. Makabe, Appl. Phys. Lett. **56**, 818 (1990).
[46]J. Schulze, E. Schüngel, Z. Donkó, D. Luggenhölscher, and U. Czarnetzki, J. Phys. D: Appl. Phys. **43**, 124016 (2010).
[47]J. B. Boffard, R. O. Jung, L. W. Anderson, and C. C. Lin, in *Advances in Atomic, Molecular, and Optical Physics*," Molecular, and Optical Physics, edited by P. R. Berman, C. C. Lin, and E. Arimondo (Elsevier, 2007), Vol. 54, pp. 319–421.
[48]J. B. Boffard, G. A. Piech, M. F. Gehrke, L. W. Anderson, and C. C. Lin, Phys. Rev. A **59**, 2749 (1999).
[49]K. H. A. Bogart and V. M. Donnelly, J. Appl. Phys. **87**, 8351 (2000).
[50]L. C. Lee, Masako Suto, and K. Y. Tang, J. Chem. Phys. **84**, 5277 (1986).
[51]U. Streller, H. Raaf, and N. Schwentner, "Light-induced dry etching of semiconductors in the vacuum ultraviolet", Proc. SPIE **3274**, (1998).
[52]Z. H. Walker and E. A. Ogryzlo, J. Appl. Phys. **69**, 548 (1991).
[53]H. F. Winters and D. Haarer, Phys. Rev. B **36**, 6613 (1987).
[54]N. Cabrera and N. F. Mott, Rep. Prog. Phys. **12**, 163 (1949).
[55]M. Arita, K. Torigoe, T. Yamauchi, T. Nagaoka, T. Aiso, Y. Yamashita, and T. Motooka, Appl. Phys. Lett. **104**, 132103 (2014).
[56]I. Vaquila, J. W. Rabalais, J. Wolfgang, and P. Nordlander, Surf. Sci. **489**, L561 (2001).
[57]I.-G. Kim, K. J. Choi, and J.-L. Lee, J. Vac. Sci. Technol. B **23**, 495 (2005).
[58]D. Troost, L. Koenders, L.-Y. Fan, and W. Mönch, J. Vac. Sci. Technol. B **5**, 1119 (1987).
[59]W. Mönch, J. Vac. Sci. Technol. B **7**, 1216 (1989).
[60]H. F. Winters, J. Vac. Sci. Technol. B **1**, 469 (1983).
[61]Y. H. Lee and M. Chen, J. Vac. Sci. Technol. B **4**, 468 (1986).
[62]C. C. Cheng, K. V. Guinn, V. M. Donnelly, and I. P. Herman, J. Vac. Sci. Technol. A **12**, 2630 (1994).
[63]N. Layadi, V. M. Donnelly, J. T. C. Lee, and F. P. Klemens, J. Vac. Sci. Technol. A **15**, 604 (1997).
[64]P. A. Tchertchian, C. J. Wagner, T. J. Houlahan, Jr., B. Li, D. J. Sievers, and J. G. Eden, Contrib. Plasma Phys. **51**, 889 (2011).
[65]A. J. Tuzzolino, Phys. Rev. **134**, A205 (1964).
[66]M. Bernardi, D. Vigil-Fowler, J. Lischner, J. B. Neaton, and S. G. Louie, Phys. Rev. Lett. **112**, 257402 (2014).
[67]W. Shockley, Czech J. Phys. **11**, 81 (1961).
[68]H. D. Hagstrum, Phys. Rev. **122**, 83 (1961).
[69]R. L. Whetten, K.-J. Fu, and E. R. Grant, J. Chem. Phys. **77**, 3769 (1982).
[70]S. Yanagida, K. Mizumoto, and C. Pac, J. Am. Chem. Soc. **108**, 647 (1986).
[71]M. W. Chase, C. A. Davies, D. J. Downey, J. R. Fruripn, and R. A. McDonald, *NIST-JANAF Thermochemical Tables*, 4th ed. (American Chemical Society, New York, 1998).
[72]C.-R. Wen and L.-C. Chou, J. Chem. Phys. **120**, 11144 (2004).
[73]R. Locht and J. Momigny, Int. J. Mass Spectrom. Ion Phys. **7**, 121 (1971).
[74]L. Šiller, S. L. Bennett, M. A. MacDonald, R. A. Bennett, R. E. Palmer, and J. S. Foord, Phys. Rev. Lett. **76**, 1960 (1996).

05 September 2023 11:49:35

Published under an exclusive license by the AVS